

CowScape: Quantitative reconstruction of the conformational landscape of biological macromolecules from cryo-EM data

Felix Lambrecht¹, Andreas Kröpelin², Mario Lüttich¹, Michael Habeck^{2,1,*},
David Haselbach^{1,3,*}, Holger Stark^{1,*}

February 20, 2024

¹Max Planck Institute for Multidisciplinary Sciences, 37077 Göttingen, Germany

²Microscopic Image Analysis Group, Jena University Hospital, 07743 Jena, Germany

³Institute for Molecular Pathology, Vienna, Austria

*E-Mail: hstark1@gwdg.de; david.haselbach@imp.ac.at; michael.habeck@uni-jena.de

Abstract

Cryo-EM data processing typically focuses on the structure of the main conformational state under investigation and discards images that belong to other states. This approach can reach atomic resolution, but ignores vast amounts of valuable information about the underlying conformational ensemble and its dynamics. CowScape analyzes an entire cryo-EM dataset and thereby obtains a quantitative description of structural variability of macromolecular complexes that represents the biochemically relevant conformational space. By combining extensive image classification with principal component analysis (PCA) of the classified 3D volumes and kernel density estimation, CowScape can be used as a quantitative tool to analyze this variability. PCA projects all 3D structures along the major modes spanning a low-dimensional space that captures a large portion of structural variability. The number of particle images in a given state can be used to calculate an energy landscape based on kernel density estimation and Boltzmann inversion. By revealing allosteric interactions in macromolecular complexes, CowScape allows us to distinguish and interpret dynamic changes in macromolecular complexes during function and regulation.

1 Introduction

Most biological processes in the cell are not driven by individual biomolecules but rather by large macromolecular assemblies comprising numerous proteins and/or nucleic acids (Gavin *et al.*, 2002). These complexes can be considered as molecular machines: they tend to be highly dynamic and undergo significant conformational rearrangements during their reaction cycles. In their natural biological context, molecular machines are regulated, for example, by the binding of external factors that restrict the conformational freedom in a functionally relevant manner. Understanding the function of macromolecular machines requires that we consider the entire conformational landscape that the macromolecular complex explores during regulation and its reaction cycle (Fischer *et al.*, 2010; Haselbach *et al.*, 2017, 2018; Singh *et al.*, 2020).

The current focus of single-particle cryo-EM is mainly on high-resolution structure determination of a single static state. Realizing the potential of single-particle cryo-EM for studying both the structure and dynamics of macromolecular machines, necessitates that we go beyond the current state-of-the-art in cryo-EM data processing. The most complete description would be a high-resolution molecular “movie” of the entire accessible conformational space. Such a movie would, for example, allow us to better understand allosteric regulation effects resulting from the binding of a ligand (such as a drug) that affects the activity of the complex.

Historically, X-ray crystallography has dominated as the method for determining high-resolution structure of macromolecular complexes. Yet X-ray crystallography is mainly limited to static structure determination, because it studies copies of the molecule in roughly the same conformation packed into a crystal lattice. Cryo-EM, in contrast, images individual molecules in a frozen hydrated state with no bias to adopt a conformation preferred by crystal packing. The range of structural heterogeneity due to conformational dynamics is therefore significantly higher in cryo-EM than in X-ray crystallography. This can be very problematic for high-resolution structure determination with cryo-EM and is reflected by the current statistics of the Electron Microscopy Data Bank (EMDB) that reveal how detrimental structural heterogeneity can be. Despite ground-breaking technical developments that now allow the determination of single-state structures up to atomic resolution, the average resolution of cryo-EM structures deposited in EMDB (The wwPDB Consortium, 2023), is significantly lower. Indeed, any mixture of conformations (due to either low sample quality or the presence of multiple conformations) will always be resolution-limiting in cryo-EM.

Some aspects of this heterogeneity can be tackled by using computational tools to sort cryo-EM images according to differences in composition and conformation. A large dataset of cryo-EM images can thus be purified *in silico* to compensate for a higher level of conformational and structural heterogeneity. Computational tools have been developed for this computational sorting, including two-dimensional (2D) PCA (Elad *et al.*, 2008), maximum likelihood-based classification in 2D/3D (Scheres, 2016; Moriya *et al.*,

2017), and manifold embedding of raw images (Dashti *et al.*, 2014). However, while these computational tools effectively distinguish between distinct conformational states of the molecules, their ability to separate continuous conformational differences is usually limited.

Currently, the most widely used classifications in cryo-EM are based on maximum-likelihood (Sigworth, 1998). They do not require prior knowledge and are easy to use via powerful software packages such as Relion (Scheres, 2016) or cryoSparc (Punjani *et al.*, 2017). A cryo-EM project typically aims to computationally purify particle images that belong to the main conformational state present in the dataset. Several rounds of classification remove particle images that do not match the main conformational state. The “purified” sub-population can then be refined to high resolution. In some cases, this approach discards more than 90% of all images to reach a level of homogeneity that allows the calculation of a high-resolution structure. Thus, the majority of images does not belong to the best sub-population in many cryo-EM datasets. The discarded data are not analyzed further, such that it remains unclear why the majority of images do not contribute to the high-resolution structure. Nonetheless, the discarded data may still contain interesting and relevant information.

In an ideal situation, the entire data would be used to computationally purify all well-defined states that exist in a given dataset, rather than only the most evident ones, and each image would be classified into its corresponding three-dimensional (3D) structure. However, such an approach would require massive image statistics, because the conformational freedom of the entire macromolecular complex should be computationally sorted to understand its full dynamics. In recent years, a number of computational tools have been developed to tackle conformational heterogeneity in cryo-EM datasets (Tang *et al.*, 2023; Toader *et al.*, 2023). These range from manifold embedding (Dashti *et al.*, 2014, 2020), to multi-body refinement (Nakane *et al.*, 2018) and machine-learning approaches (Chen and Ludtke, 2021; Zhong *et al.*, 2021), to name just a few.

The first attempt to determine the entire conformational landscape from a large image dataset was the exhaustive computational analysis of an *E. coli* 70S ribosome trapped in intermediate states of tRNA retro-translocation (Fischer *et al.*, 2010). In this study, two million particle images were used to separate 50 conformational states by a hierarchical computational purification procedure as well as by visual inspection of the calculated 3D structures based on the tRNA positions on the ribosome. Following the tRNA motions by visual comparison of all structures allowed the order of the structures to be determined along a conformational trajectory. After taking the particle statistics into account, the first energy landscape based on cryo-EM data was determined (Fischer *et al.*, 2010). The entire procedure required extensive manual image processing, as well as prior knowledge about tRNA motions, to find the order of all states which was later confirmed by molecular dynamic simulations (Bock *et al.*, 2013). It is therefore impractical to apply this approach to samples for which little or no prior knowledge is available.

Despite the recent progress in addressing continuous conformational heterogeneity

in cryo-EM datasets (Tang *et al.*, 2023; Toader *et al.*, 2023), we prefer a conceptually simple and interpretable approach that does not require exhaustive training, but can be applied directly to any dataset. To realize this idea, we have developed CowScape, a computational approach to obtain a quantitative description of conformational variability of macromolecular complexes (Fig. 1a). CowScape combines extensive maximum-likelihood 3D classification and PCA (3D-PCA) to determine all possible conformational states without the need for any prior knowledge about the complexes. PCA is used in several approaches to analyze heterogeneity in cryo-EM (e.g. by Tagare *et al.* (2015) as well as Punjani and Fleet (2021)). Despite its limitations in resolution (Sorzano and Carazo, 2021), we find that 3D-PCA is a highly useful tool to study large-scale conformational changes, in particular when combined with biochemical knowledge. CowScape analyzes the similarities and differences of the states in a meaningful and automated manner and then orders the states by a PCA of all calculated and aligned 3D volumes. The number of states can range from several tens to several hundreds of structures. The main modes of conformational variations are directly obtained by the major PCA eigenvectors (Fig. 1b). Taking two major modes allows the conformational landscape to be plotted, which provides a plausible trajectory of conformational changes (Fig. 1c). Furthermore, the number of particle images used to calculate the structures of each conformational state is known. Based on the particle numbers, CowScape can convert the conformational landscape into an energy landscape by applying Boltzmann's law. We have applied CowScape to large macromolecular complexes including the human 26S proteasome (Haselbach *et al.*, 2017), the human B-act spliceosome (Haselbach *et al.*, 2018) and the fatty acid synthase (Singh *et al.*, 2020). In all cases, CowScape allowed us to determine structures of unknown conformations and obtain new structural insight into functionally relevant regulatory mechanisms. Here, we present the details of how CowScape works and a demonstration of its general applicability.

2 Results

The CowScape algorithm is available in the COW image processing suite (www.cow-em.de). CowScape provides tools for 3D classification and refinement, the generation of conformational ensembles and energy landscapes, for plotting data as a 2D heat map, and for visualizing these data as a 3D landscape. The first step is an extensive 3D classification of all data identified as true particle images within a cryo-EM dataset (for an overview see Fig. 1). 3D classification can be performed with various image processing packages (Scheres, 2016; Moriya *et al.*, 2017; Grant *et al.*, 2018; Punjani *et al.*, 2017) including the COW package. After classification, each sub-population is refined to the highest possible resolution. Notably, 3D classification provides both an overview of the conformational ensemble and the number of particles assigned to each class. These numbers encode highly valuable quantitative information, because a thermodynamically stable conformation will be observed with a higher particle frequency than a thermody-

namically less-favored state. The particle number per conformational sub-population thus directly translates into free energy differences and can be used to construct an energy landscape via Boltzmann inversion (see Supplementary Methods).

3D classification provides a large number of structures in different conformations and the corresponding particle numbers that were used to calculate the structures. However, at this stage, the set of 3D structures lacks any order relative to each other; instead, it simply reflects the conformation ensemble present in the dataset. To obtain a quantitative description of the major structural similarities, all 3D structures are subjected to 3D-PCA. 3D-PCA yields the eigenvectors (3D volumes) that capture the structural variances in a hierarchical manner. Typically, the first few eigenvolumes can be used to describe a large part of the heterogeneity in the dataset. CowScape uses this information to visualize continuous motions along the first eigenvectors in a movie-like manner. These animations can reveal the major modes of motion present in the dataset and the coupling of movable parts in the macromolecular complex. The major eigenvectors may also serve as coordinate axes that span an energy landscape. The energy landscape can be visualized as a heatmap, the colors indicate the relative Gibbs free-energy differences (Fig. 2). All classified 3D structures can be mapped into the coordinate system (i.e. on top of the energy heatmap) that describes the major conformational variability. The energy profile provides the user with valuable information about the number of conformational states and an estimate of the energy barriers separating them.

CowScape is generally applicable as demonstrated by previous studies of the 26S proteasome (Haselbach *et al.*, 2017), the human spliceosome (Haselbach *et al.*, 2018) and the fatty acid synthase (Singh *et al.*, 2020). We have also demonstrated its use on publicly available cryo-EM datasets in the Electron Microscopy Public Image Archive (EMPIAR) database (Supplementary Methods). These datasets also serve as additional examples of what can be learned from a CowScape analysis. All datasets were downloaded and processed in a similar manner (see Methods). The 3D volumes were subjected to 3D-PCA, and the corresponding energy landscapes were calculated (Fig. 2) by Kernel Density Estimation with a Gaussian kernel function (Supplementary Methods).

Some general features of macromolecular complexes can be seen directly in the energy landscape plots (Fig. 3). For some biochemically well-behaved complexes, such as the non-selective cation channel TRPM4 (Fig. 4), the energy landscape reveals well-defined thermodynamic minima (blue), suggesting that a large part of the data contributes to one major structure, and that there is only a relatively small number of distinct states in the dataset. In contrast, other complexes such as the spliceosome reveal a continuously populated energy landscape, making it more difficult to find a sufficient number of images to determine structures of all conformational states at high resolution. For these complexes, the energy barriers between the various states are much smaller, and the energy landscape can usually be modulated more easily by ligands that bind to the complex.

It is also noteworthy that, depending on the nature of the macromolecular complex,

the energy landscape not only reflects the conformational heterogeneity of the complex, but can also contain sub-populations of complexes that differ in their composition. CowScape always analyzes the entire variability in the dataset, which comprises both conformational and compositional heterogeneity. If the sample is known to be a very clean preparation, the population landscapes can be interpreted as differences in conformational sampling of the same complex, and thus assumed to correspond to an energy landscape. In either case, the landscape provides the user with the unique possibility of discovering previously unknown conformations, for which one can subsequently try to select the raw data and refine them to high-resolution. For instance, the landscape determined for the mitotic checkpoint complex (MCC) bound to the anaphase promoting complex (APC) (Brown *et al.*, 2016) revealed a high level of biochemical heterogeneity within the complex. Therefore, Fig. 2 cannot be interpreted as an energy landscape. The two major eigenvectors of this dataset describe the stable integration of MCC into the APC complex and the presence or absence of the protein APC2. Such a landscape can thus be used as a tool to quantitatively monitor any improvement in complex preparation and purification, with the goal of maximizing the number of molecules that integrate all desired components stably into the complex. Energy landscapes can only be determined at a later stage after successful biochemical optimization.

To focus on conformational variability, we analyzed examples that can be considered being biochemically optimized, namely, the 26S proteasome and the TRPM4 channel 16 (Figs. 3 and 4). For the 26S proteasome (Fig. 3), our analysis confirmed the macromolecular complex conformations that had been previously described (Lu *et al.*, 2017; Wang *et al.*, 2017). However, the energy landscapes provided a more quantitative view about the data in general that goes beyond previous findings. Specifically, we applied CowScape to two highly dynamic proteasome samples, focusing on the subunit RPN1 within the 26S proteasome holocomplex (Fig. 3a) and the regulatory 19S subcomplex bound to the chaperone p28 (Fig. 3b). A focused classification and subsequent CowScape analysis revealed an almost continuous pendulum-like motion for RPN1, which would explain why this protein has so far been elusive in high-resolution structure studies of the 26S proteasome. The pendulum-like two-state distribution has its pivot point within the N-terminal coiled coil of RPT1 and RPT2 and might represent a regulatory mechanism by which the Rpt1/2 interface can be blocked (Supplementary Fig. S1).

In contrast to other observed motions, the mobility of the RPN1 pendulum does not seem to be directly coupled to the larger modes of motion that can be observed for the entire 26S proteasome. For the 19S proteasome, we observed opening of the Rpt2/Rpt6 interface in the ATPase ring structure with a simultaneous closing of the Rpt3/4 interface. These changes correlate with a second interface closure at the RPN3 / RPN7 interface in the non-ATPase part of the complex (Supplementary Fig. S2). Thus, using CowScape we can not only automatically recover the order of minimum changes through the conformational snapshots but also directly distinguish between non-coupled and coupled motions within a macromolecular complex, which is likely to provide valuable information

about the function of these large assemblies.

Figure 4 shows another striking case for the TRPM4 channel with and without bound calcium ions (EMPIAR-10127 and EMPIAR-10126, respectively) (Autzen *et al.*, 2018). We detected an interesting conformational flexibility at the cytoplasmic side of the channel, which to our knowledge has not yet been described in the literature (Fig. 4b, Supplementary Fig. S3). By comparing the landscape with and without bound calcium, we can speculate that calcium binding increases the number of contact sites between the soluble channel parts with the central coiled coil. These soluble parts might be involved in second messenger signalling, and increased flexibility might hence precede channel opening. The location of calcium binding is significantly distant from the detected conformational changes, which implies allosteric signalling. The functional relevance of these changes in conformation sampling after binding small ligands has yet to be determined.

We previously showed for the 26S proteasome that the major conformation of the entire complex was almost identical irrespective of the presence or absence of the cancer drug oprozomib (Haselbach *et al.*, 2017). However, after drug binding to the 26S proteasome, the overall conformational space differed considerably (Haselbach *et al.*, 2017). A similar situation was observed for the TRPM4 channel. Calcium binding to the TRPM4 channel is analogous to oprozomib binding to the 26S proteasome, with direct consequences on the ability of the large macromolecular complex to adopt the set of conformations that are relevant for its function. While the exact details of how this happens are still not known, it is possible to study such effects by calculating energy landscapes based on the analyses of all particle images present in a given dataset. This also implies that CowScape is a powerful tool for the structural interpretation of ligand binding to a macromolecular complex and for allowing functionally relevant conformational changes to be observed that would otherwise remain invisible (e.g., if they do not affect the stability of the major conformation).

The above examples illustrate that the quantitative analysis of conformational sampling is even more informative when two or more energy landscapes of the same complex but under different biochemical conditions can be compared. Such comparative studies are ideally suited for elucidating how regulatory factors influence macromolecular machines in a more quantitative manner. However, as analysis requires a minimal particle image frequency for a conformational state to be discovered, short-lived intermediates of a macromolecular complexes (such as those in transition states in catalysis) will not show up in this analysis, as they are not sufficiently populated. How sensitive CowScape can become at visualizing the conformational variability in macromolecular complexes in a quantitative manner will depend on the image statistics used for the CowScape analysis and on the power of the applied 3D classification algorithms and the computational processing strategy. While this may be a limitation at the moment, one can expect that detectors and computers become significantly faster in the near future, and that novel 3D classification algorithms can be developed that will be able to determine ever smaller conformational differences. The CowScape algorithm itself is very fast and will not be a

limiting factor.

3 Discussion

CowScape offers a comprehensive way to analyze and display “motions” in a cryo-EM dataset and to estimate quantitative free energy differences that can be used to deduce mechanisms underlying motions or allosteric signal propagation (Bahar *et al.*, 2010). CowScape does not need any a priori information. This makes it possible to use CowScape at a very early stage of a project, thereby allowing the identification of the macromolecular complex conformations for which high-resolution structure refinement is best possible. The kind of insight generated by CowScape goes beyond the purely structural point of view. It gains information that is comparable with, for instance, spectroscopic data, for which the distribution of states is usually accessed by only a one-dimensional output. This powerful feature of the CowScape analysis is strongly coupled to the idea of not discarding any true particle images from a given dataset. In contrast, all the available data are used to obtain a quantitative understanding of the ensemble. In the future, this may facilitate detailed quantitative experiments that describe how variables (e.g., temperature, pH values, salt conditions, or specific drugs) interfere with a macromolecular complex. It will be difficult to obtain this information by any other method, yet such insight is critical for our understanding of how large macromolecular complexes act as “molecular machines”.

Funding

This work was funded by a grant of the Deutsche Forschungsgemeinschaft (DFG) within SFB 860 to HS. MH, HS and AK are grateful for the support of the DFG within project 432680300 - SFB 1456 subproject A05. MH and AK gratefully acknowledge funding by the Carl Zeiss Foundation within the program “CZS Stiftungsprofessuren”.

Figures

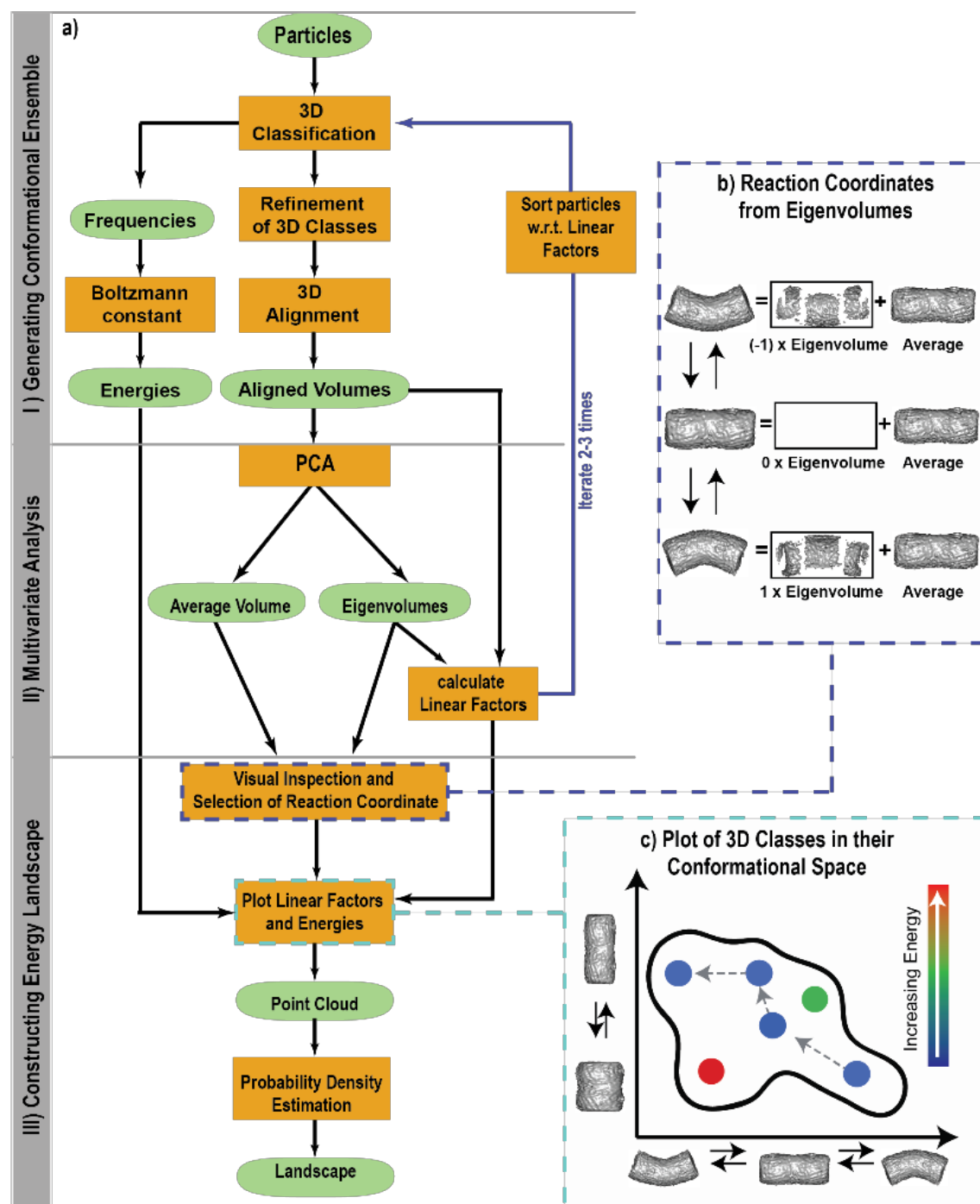


Figure 1: **The CowScape algorithm.** a) Overview of the algorithm. CowScape is roughly divided into three steps: I) generate the conformational ensemble by applying classification algorithms; II) carry out PCA; and III) make a final selection of reaction coordinates and construct the energy landscape. b) Interpretation of eigenvolumes. Each volume of a trajectory (left column) can be described as a linear combination of the eigenvolume multiplied with a linear factor and the average volume. Hence, each eigenvolume describes a conformational motion. c) Using the linear factors, volumes can be plotted into a 2D conformational space with the respective energies (indicated by a colour gradient)

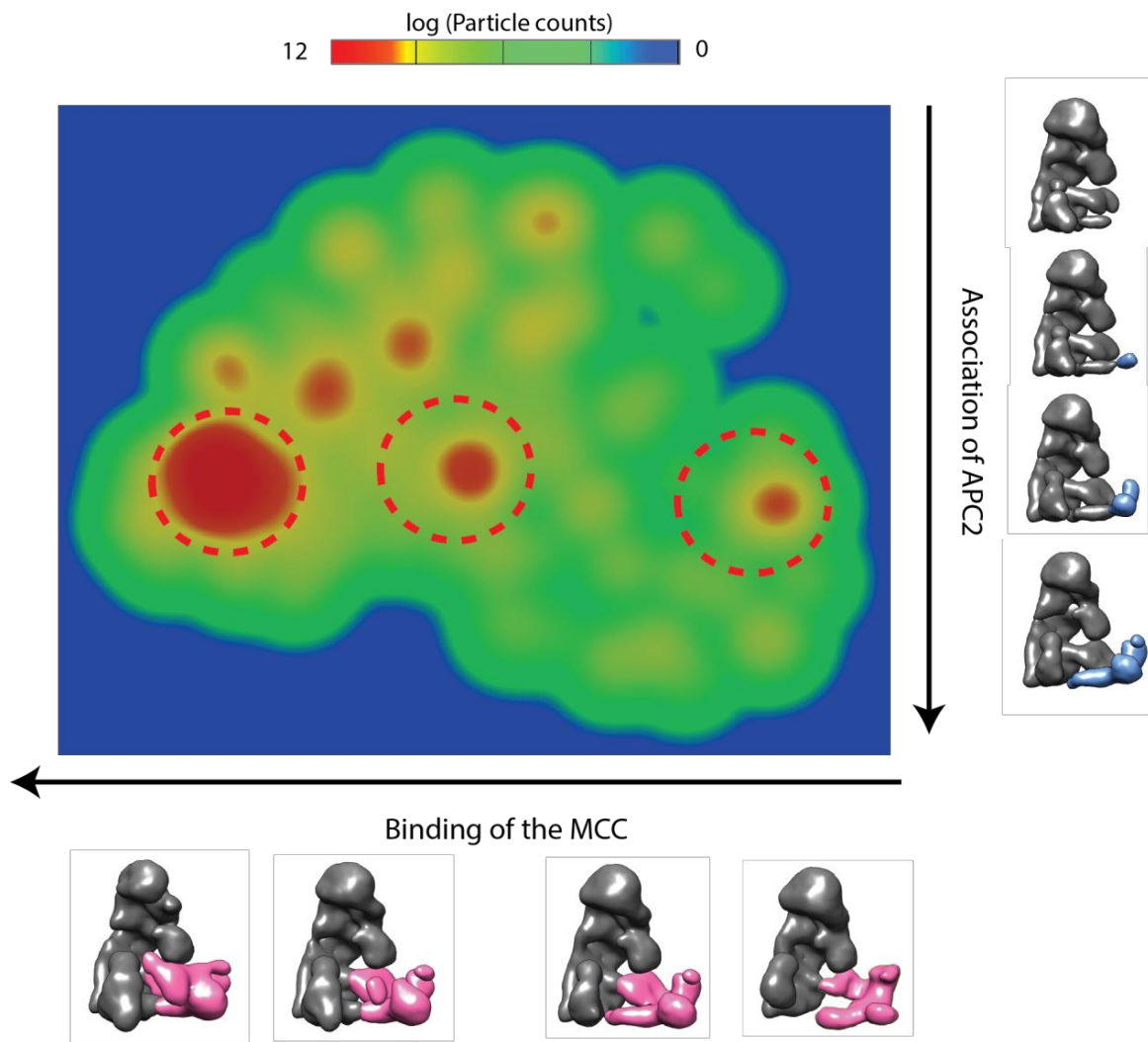


Figure 2: **Compositional landscape of APC.** This mainly compositional landscape visualizes the different assembly states of APC in a sample with a large degree of biochemical heterogeneity (i.e., it is not yet optimized in an early state of the project). The three major maxima correspond (red circles) to the different binding states of MCC (along the x-axis; shown in magenta). Any structural changes along this x-axis correspond to compositional heterogeneity of MCC binding as well as to some motion of the MCC towards the active center of the APC. The y-axis reveals the level of substoichiometric binding of the protein APC2 (shown in blue). The plot can be used as a quantitative tool to monitor and improve the biochemistry of complex purification and preparation. As such, it cannot be interpreted as an energy landscape, yet it still provides valuable information about the quality of the complex to be studied.

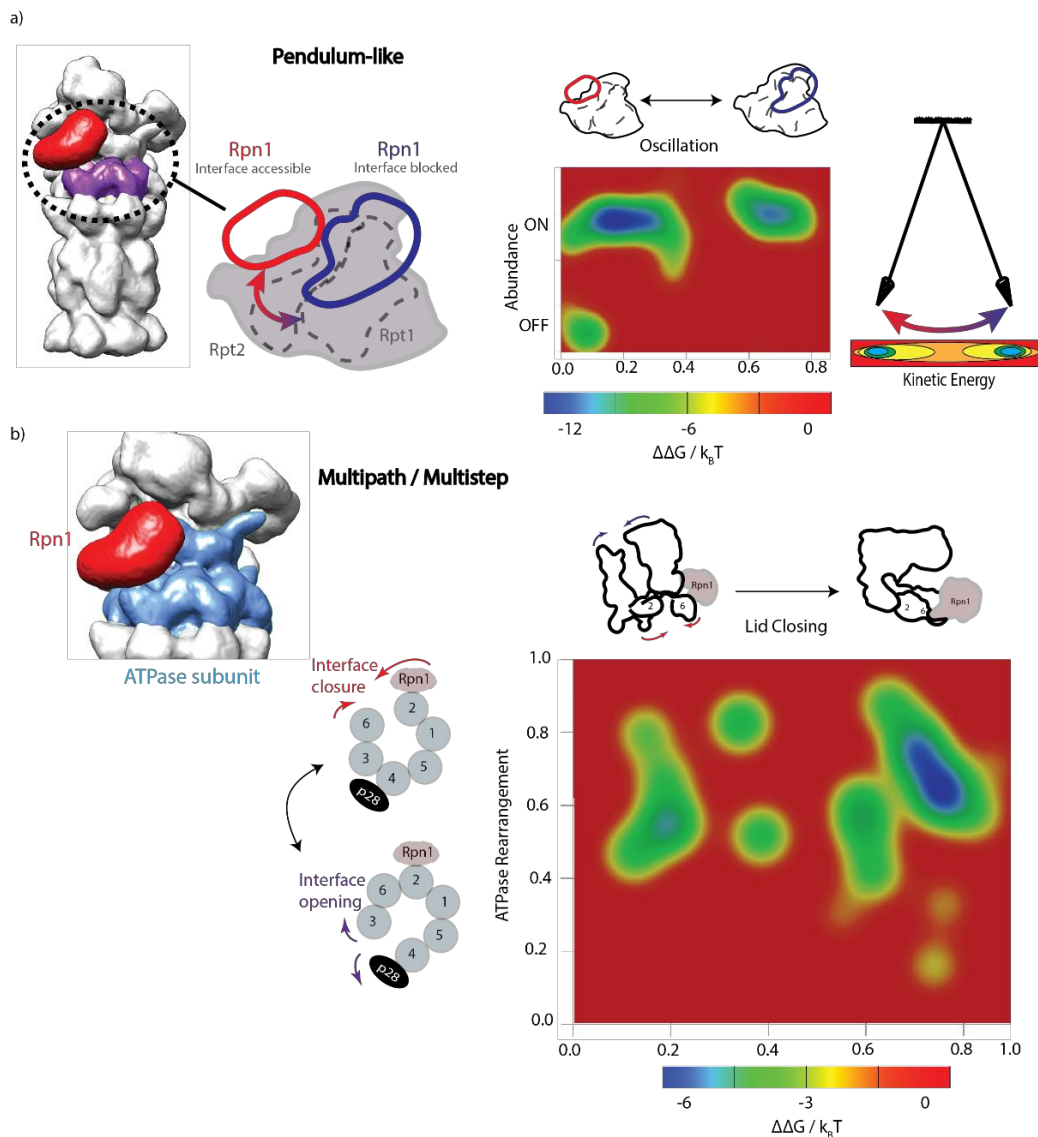


Figure 3: **Dynamic aspects within the 26S Proteasome.** a) RPN1 is a very dynamic protein that can adopt various conformations on the 26S proteasome. CowScope analysis reveals the two major conformations of RPN1 with respect to the Rpt2/Rpt1 interface (purple) and a requirement for a pendulum-like motion in order to proceed from one major state to the other. The major variability along the x-axis of the energy landscape can be described by this pendulum-like movement (see also Supplementary Fig. 1) whereas the y-axis in the plot describes RPN1 abundance. The RPN1-ON state reveals an energy profile similar to a two-state energy profile of a pendulum, as schematically depicted. b) Detailed analysis of the dynamic behaviour of the ATPase subunit (blue) as a major component of the 19S regulatory subunit of the 26S proteasome. Whereas the major mode describes an opening and closing of the 19S subunit along the x-axis of the plot, the y-axis reveals a novel conformational change in the ATPase subunit that can be summarized as an opening and closing of the ATPase ring system via different subunit interfaces.

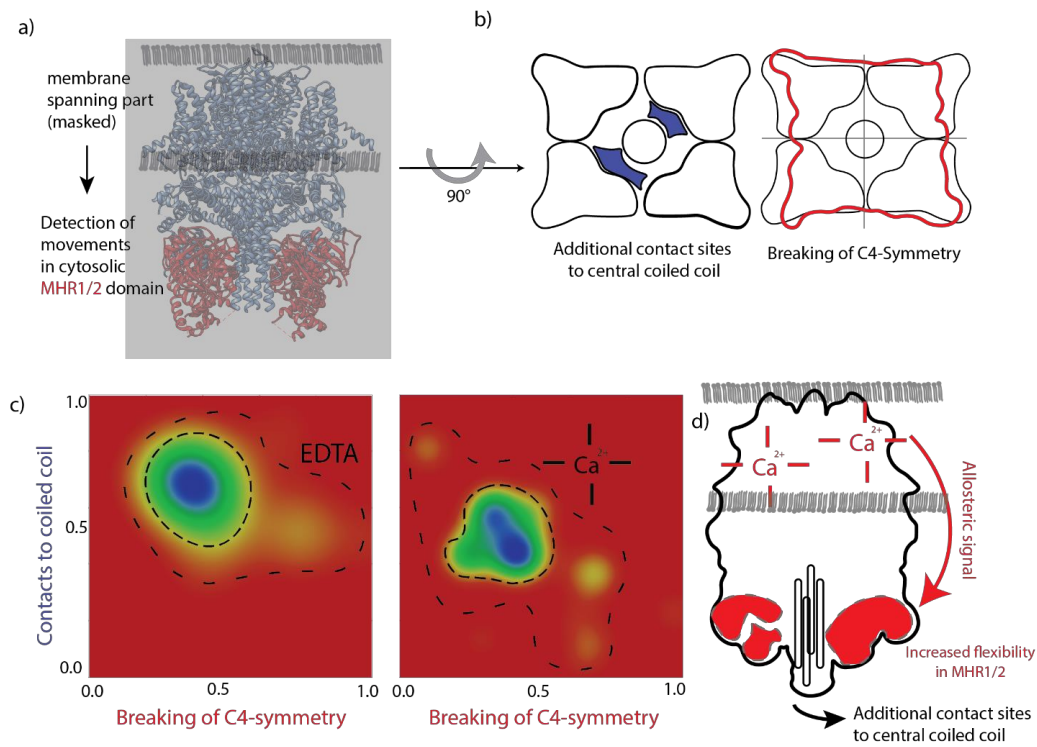


Figure 4: **Allosteric Ca^{2+} signaling in the TRPM4 channel.** a) CowScope analysis of the TRPM4 (transient receptor potential melastatin member 4) channel not only revealed the overall conformations 16 but also conformational variations that can be attributed to an overall change from a C4 to a (more-or-less) C2 symmetry behaviour (x-axis). Changes along the y-axis can be described by additional contact sites of the MHR1/2 domains being established to the central coiled-coil domain. b) Binding of calcium leads to an overall change in symmetry and to a conformational change that creates new internal contact sites. c) Even though the binding sites for calcium is on the membrane site, an increased flexibility of the MHR1/2 domains located at the opposite site can be observed, strongly suggesting that an allosteric signaling (d) pathway affects the entire TRPM4 channel and finally leads to channel opening.

References

- Autzen, H. E., Myasnikov, A. G., Campbell, M. G., Asarnow, D., Julius, D., and Cheng, Y. (2018). Structure of the human TRPM4 ion channel in a lipid nanodisc. *Science*, **359**(6372), 228–232.
- Bahar, I., Lezon, T. R., Yang, L.-W., and Eyal, E. (2010). Global dynamics of proteins: bridging between structure and function. *Annual review of biophysics*, **39**, 23–42.
- Bock, L. V., Blau, C., Schröder, G. F., Davydov, I. I., Fischer, N., Stark, H., Rodnina, M. V., Vaiana, A. C., and Grubmüller, H. (2013). Energy barriers and driving forces in tRNA translocation through the ribosome. *Nature Structural & Molecular Biology*, **20**(12), 1390–1396.
- Brown, N. G., VanderLinden, R., Watson, E. R., Weissmann, F., Ordureau, A., Wu, K.-P., Zhang, W., Yu, S., Mercredi, P. Y., Harrison, J. S., Davidson, I. F., Qiao, R., Lu, Y., Dube, P., Brunner, M. R., Grace, C. R. R., Miller, D. J., Haselbach, D., Jarvis, M. A., Yamaguchi, M., Yanishevski, D., Petzold, G., Sidhu, S. S., Kuhlman, B., Kirschner, M. W., Harper, J. W., Peters, J.-M., Stark, H., and Schulman, B. A. (2016). Dual RING E3 architectures regulate multiubiquitination and ubiquitin chain elongation by APC/C. *Cell*, **165**(6), 1440–1453.
- Chen, M. and Ludtke, S. J. (2021). Deep learning-based mixed-dimensional gaussian mixture model for characterizing variability in cryo-em. *Nature Methods*, **18**(8), 930–936.
- Dashti, A., Schwander, P., Langlois, R., Fung, R., Li, W., Hosseinizadeh, A., Liao, H. Y., Pallesen, J., Sharma, G., Stupina, V. A., *et al.* (2014). Trajectories of the ribosome as a Brownian nanomachine. *Proceedings of the National Academy of Sciences*, **111**(49), 17492–17497.
- Dashti, A., Mashayekhi, G., Shekhar, M., Ben Hail, D., Salah, S., Schwander, P., des Georges, A., Singharoy, A., Frank, J., and Ourmazd, A. (2020). Retrieving functional pathways of biomolecules from single-particle snapshots. *Nature Communications*, **11**(1), 4734.
- Elad, N., Clare, D. K., Saibil, H. R., and Orlova, E. V. (2008). Detection and separation of heterogeneity in molecular complexes by statistical analysis of their two-dimensional projections. *Journal of Structural Biology*, **162**(1), 108–120.
- Fischer, N., Konevega, A. L., Wintermeyer, W., Rodnina, M. V., and Stark, H. (2010). Ribosome dynamics and trna movement by time-resolved electron cryomicroscopy. *Nature*, **466**(7304), 329–333.

- Gavin, A.-C., Bösche, M., Krause, R., Grandi, P., Marzioch, M., Bauer, A., Schultz, J., Rick, J. M., Michon, A.-M., Cruciat, C.-M., Remor, M., Höfert, C., Schelder, M., Brajenovic, M., Ruffner, H., Merino, A., Klein, K., Hudak, M., Dickson, D., Rudi, T., Gnau, V., Bauch, A., Bastuck, S., Huhse, B., Leutwein, C., Heurtier, M.-A., Copley, R. R., Edelman, A., Querfurth, E., Rybin, V., Drewes, G., Raida, M., Bouwmeester, T., Bork, P., Seraphin, B., Kuster, B., Neubauer, G., and Superti-Furga, G. (2002). Functional organization of the yeast proteome by systematic analysis of protein complexes. *Nature*, **415**(6868), 141–147.
- Grant, T., Rohou, A., and Grigorieff, N. (2018). cisTEM, user-friendly software for single-particle image processing. *elife*, **7**, e35383.
- Haselbach, D., Schrader, J., Lambrecht, F., Henneberg, F., Chari, A., and Stark, H. (2017). Long-range allosteric regulation of the human 26s proteasome by 20s proteasome-targeting cancer drugs. *Nature communications*, **8**(1), 15578.
- Haselbach, D., Komarov, I., Agafonov, D. E., Hartmuth, K., Graf, B., Dybkov, O., Urlaub, H., Kastner, B., Lührmann, R., and Stark, H. (2018). Structure and conformational dynamics of the human spliceosomal bact complex. *Cell*, **172**(3), 454–464.
- Lu, Y., Wu, J., Dong, Y., Chen, S., Sun, S., Ma, Y.-B., Ouyang, Q., Finley, D., Kirschner, M. W., and Mao, Y. (2017). Conformational landscape of the p28-bound human proteasome regulatory particle. *Molecular Cell*, **67**(2), 322–333.
- Moriya, T., Saur, M., Stabrin, M., Merino, F., Voicu, H., Huang, Z., Penczek, P. A., Raunser, S., and Gatsogiannis, C. (2017). High-resolution single particle analysis from electron cryo-microscopy images using sphire. *JoVE (Journal of Visualized Experiments)*, **123**, e55448.
- Nakane, T., Kimanius, D., Lindahl, E., and Scheres, S. H. (2018). Characterisation of molecular motions in cryo-EM single-particle data by multi-body refinement in RELION. *elife*, **7**, e36861.
- Punjani, A. and Fleet, D. J. (2021). 3d variability analysis: Resolving continuous flexibility and discrete heterogeneity from single particle cryo-em. *Journal of Structural Biology*, **213**(2), 107702.
- Punjani, A., Rubinstein, J. L., Fleet, D. J., and Brubaker, M. A. (2017). cryoSPARC: algorithms for rapid unsupervised cryo-EM structure determination. *Nature Methods*, **14**(3), 290–296.
- Scheres, S. H. (2016). Processing of structurally heterogeneous cryo-em data in relion. *Methods in Enzymology*, **579**, 125–157.
- Sigworth, F. J. (1998). A maximum-likelihood approach to single-particle image refinement. *Journal of Structural Biology*, **122**(3), 328–339.

- Singh, K., Graf, B., Linden, A., Sautner, V., Urlaub, H., Tittmann, K., Stark, H., and Chari, A. (2020). Discovery of a regulatory subunit of the yeast fatty acid synthase. *Cell*, **180**(6), 1130–1143.
- Sorzano, C. O. S. and Carazo, J. M. (2021). Principal component analysis is limited to low-resolution analysis in cryoEM. *Acta Crystallographica Section D*, **77**(6), 835–839.
- Tagare, H. D., Kucukelbir, A., Sigworth, F. J., Wang, H., and Rao, M. (2015). Directly reconstructing principal components of heterogeneous particles from cryo-em images. *Journal of Structural Biology*, **191**(2), 245–262.
- Tang, W. S., Zhong, E. D., Hanson, S. M., Thiede, E. H., and Cossio, P. (2023). Conformational heterogeneity and probability distributions from single-particle cryo-electron microscopy. *Current Opinion in Structural Biology*, **81**, 102626.
- The wwPDB Consortium (2023). EMDB—the Electron Microscopy Data Bank. *Nucleic Acids Research*, **52**(D1), D456–D465.
- Toader, B., Sigworth, F. J., and Lederman, R. R. (2023). Methods for cryo-em single particle reconstruction of macromolecules having continuous heterogeneity. *Journal of Molecular Biology*, **435**(9), 168020.
- van Heel, M., Portugal, R. V., Schatz, M., *et al.* (2016). Multivariate statistical analysis of large datasets: Single particle electron microscopy. *Open Journal of Statistics*, **6**(04), 701.
- Wang, X., Cimermancic, P., Yu, C., Schweitzer, A., Chopra, N., Engel, J. L., Greenberg, C., Huszagh, A. S., Beck, F., Sakata, E., Yang, Y., Novitsky, E. J., Leitner, A., Nanni, P., Kahraman, A., Guo, X., Dixon, J. E., Rychnovsky, S. D., Aebersold, R., Baumeister, W., Sali, A., and Huang, L. (2017). Molecular details underlying dynamic structures and regulation of the human 26s proteasome. *Molecular & Cellular Proteomics*, **16**(5), 840–854.
- Zhong, E. D., Bepler, T., Berger, B., and Davis, J. H. (2021). Cryodrgn: reconstruction of heterogeneous cryo-em structures using neural networks. *Nature Methods*, **18**(2), 176–185.

Supplementary Figures

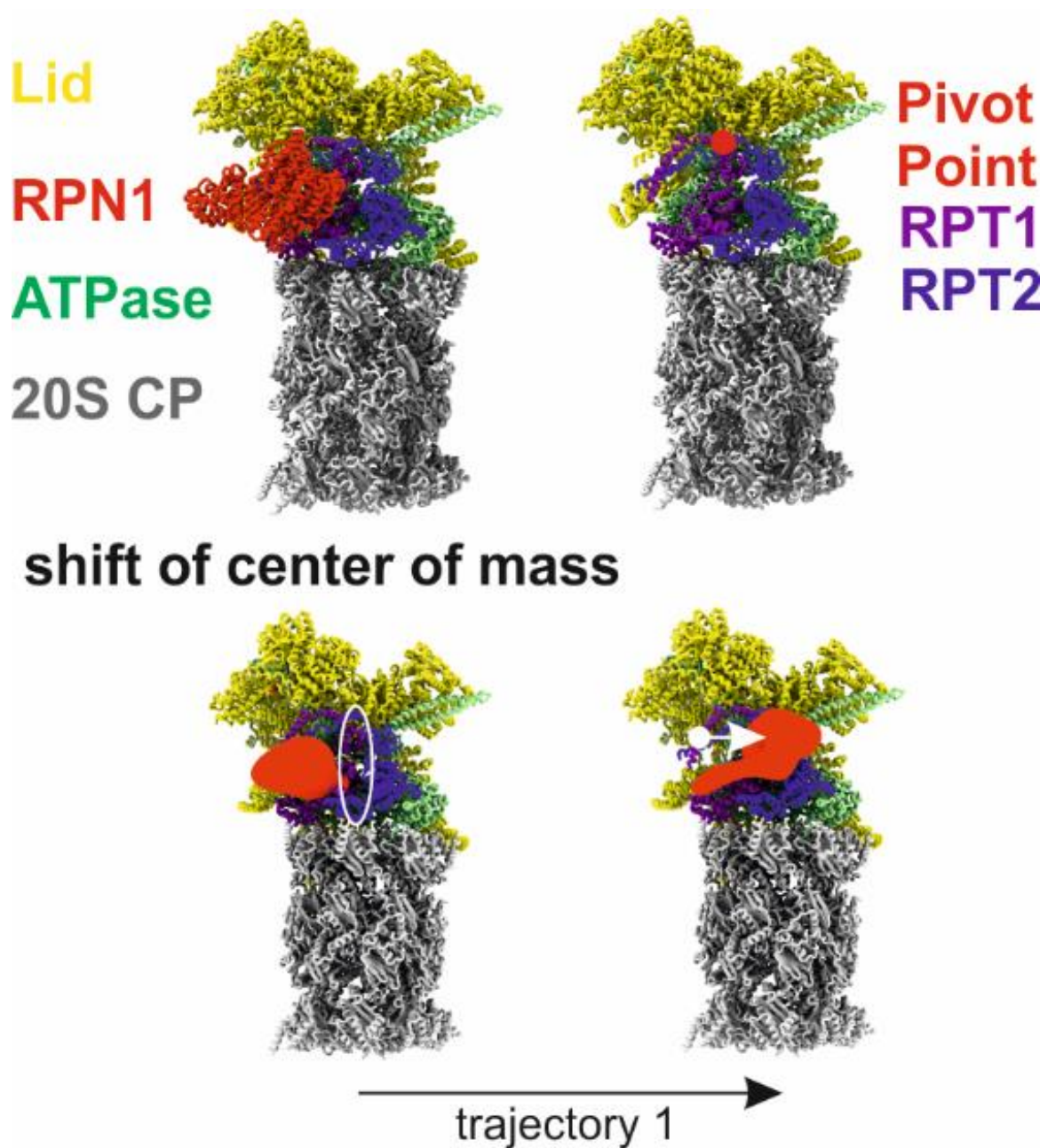
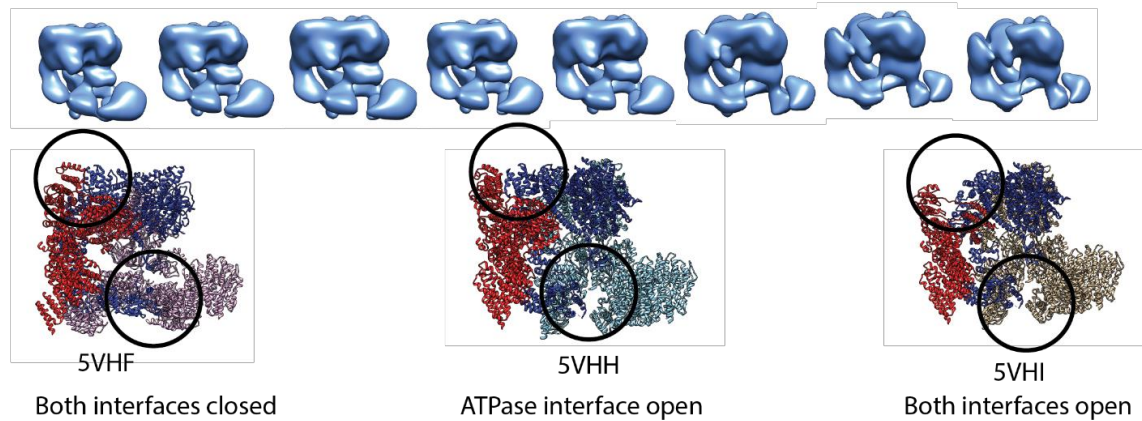


Figure S1: **RPN1 movement.** The upper panel shows the same view of the human 26S Proteasome (PDB 5M32) with and without the protein RPN1. RPN1 is labelled in red and the proteins RPT1 and RPT2 are coloured in purple and blue, respectively. CowScape revealed a combined shift and pendulum-like movement of RPN1 described in the main text that reflects the major variability along the first eigenvector. RPN1's center of mass completely covers the RPT1/2 interface (white circle). RPN1 shifts from its position in front of RPT1 (white dot) towards RPT2 following the indicated movement vector.

a) Lid Closing



b) ATPase Rearrangement

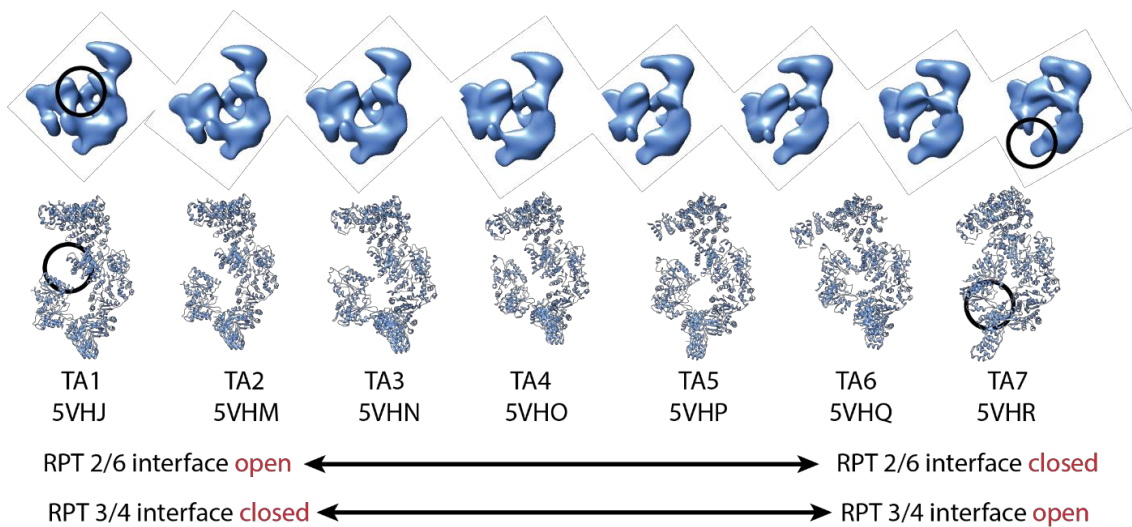


Figure S2: **p28-bound 19S proteasome**. Binding of p28 is a necessary component of the 26S assembly pathway, as it positions the 19S correctly on the 20S core particle, to form the full 26 proteasome. CowScape detected – automatically and without a priori information – the findings described by Lu *et al.* (2017). a) The results of the PCA analysis confirm the lid closing observed by Lu *et al.* b) Using CowScape we determined another motion located in the ATPase ring system that correlates with the lid closing. Here we observe an alternating opening of the RPT2/6 and RPT3/4 interfaces. Based on the energy landscape shown in Fig. 3, we can conclude that the lid closes upon p28 binding. Simultaneously, the ATPase interface changes in going from an open RPT2/6 interface to an open RPT3/4 interface.

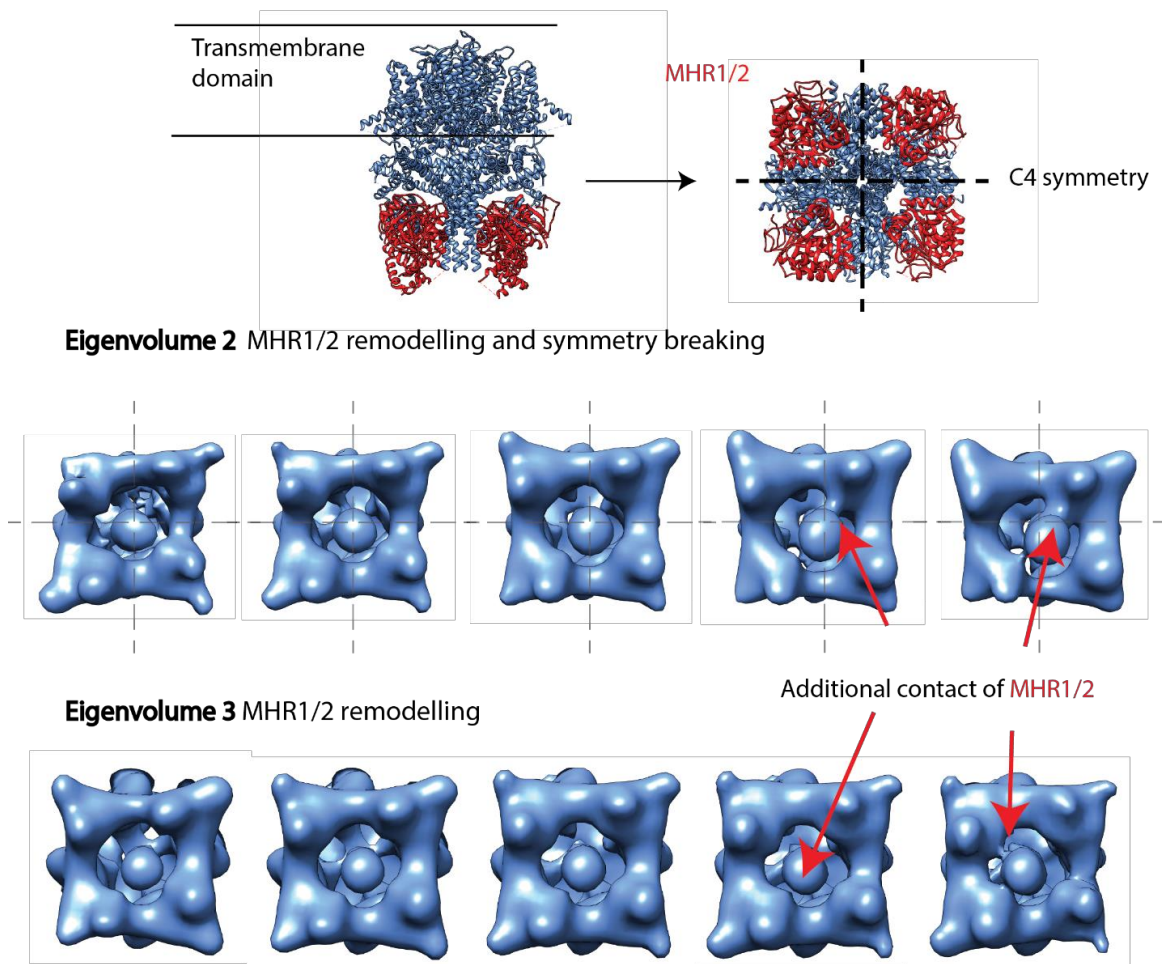


Figure S3: **Analysis of motions in the TRPM4 channel.** TRPM4 has been implicated in various severe diseases, such as diffuse large B-cell lymphomas and complete heart block. Our analysis focused on the cytoplasmic domain by applying a mask during PCA. Additionally, we did not restrict our analysis to C4 symmetry. The original structure (6BQV) is shown in the upper panel, with the MHR1/2 domains marked in red. We detected large symmetry breaks in the second eigenvolume as well as additional contact sites of the MHR1/2 domains with the central coiled coil in the eigenvolumes 2 and 3. These contact sites were not observed in the original analysis by Autzen *et al.* (2018). Interestingly, the MHR1/2 domains harbour putative binding sites for secondary messengers, such as PIP2 and PIP3. Flexibility seems to increase upon binding of calcium ions, which precedes channel opening. The observed additional binding sites to the coiled-coil might be the reason why Autzen *et al.* observed more side chains to be visible in the calcium bound state.

A Data analysis

All data were downloaded from the EMPIAR Database (Spliceosome: 10160, Proteasome: 10166, 19S particle with p28: 10091 and the TRPM4 channel 10126, 10127) and subjected to several rounds of 2D classification in the COW suite to remove non-particle views. As described in the main text, the general workflow divides into three main parts:

1. The generation of an ensemble of 3D structures.
2. The calculation and visual inspection of the reaction coordinates.
3. The construction of the energy landscape.

B Ensemble Generation and Alignment

We define an *ensemble* as a set of 3D volumes of the same size and voxel size. Our approach can be applied to any conformational ensemble of 3D volumes. Here, we describe an application to 3D volumes generated by extensive Maximum-Likelihood 3D classification, which is tested in RELION, SPHIRE and the COW Suite. For all examples discussed in the manuscript, classes were prepared with classification runs containing 200,000 particles on 40 classes (if the initial dataset was smaller, fewer classes were used so as to match the same ratio between the number of particles and the number of classes). It is necessary to split the entire population of particles into multiple batches which are classified separately, because the computational effort increases dramatically with the number of particles. After classification, individual volumes were autorefined and all volumes were pooled into a single ensemble. Because PCA is sensitive to any difference between the volumes, aligning them against the same reference is crucial. This alignment was carried out either in the COW Suite using the Logic *3DAlignment* with standard parameters or in UCSF Chimera with the *FitinMap* procedure. *3DAlignment* maximizes the real space cross-correlation coefficient to a reference by applying shifts and rotations to the volume. Some remarks regarding the specifics of processing the data sets are listed below:

Dataset	Remarks on classification and processing
26S/rpn1	No alignment was necessary, because the classification was only local and the 20S part remained stable throughout the classification runs.
TRPM4	The classification and subsequent refinement was performed without applying symmetry restraints (in contrast to the original publication).

All subsequent steps were performed within *CowEyes*. The volumes were lowpass-filtered to the lowest resolution among all ensemble members. This is necessary to avoid

that PCA picks up resolution differences between the volumes. The Fourier space cutoff of the filter is given by

$$\gamma = \frac{2 \times \text{pixelSize}}{\text{lowest resolution}}$$

Subsequently, all volumes were normalized to a mean of zero and a standard deviation σ of 2. The parameter σ is an important variable to fine-tune the information content of the eigenvolumes, as it directly influences the detection of information by PCA in the next step.

C Principal Component Analysis (PCA)

PCA finds an embedding of the input data in a lower dimensional space that preserves the correlation structure of the data as much as possible (for a thorough review of PCA see van Heel *et al.* (2016)). The coordinate axes of the lower dimensional space are obtained by calculating the eigenvectors of the covariance matrix of the input data (the ensemble of volumes). The eigenvectors are orthogonal to each other and sorted by the amount of covariance that each of them represents (their corresponding eigenvalue). CowEyes' implementation of PCA is memory efficient especially for large volumes, since it uses the dimensional $N \times N$ covariance matrix where N is the number of volumes. By selecting a subset of the eigenvectors we construct a lower dimensional space that represents the input. The position of the volume in this lower-dimensional space is determined by a vector of linear factors a where a_n (representing the n -th volume) has as many entries as the dimensionality of the embedding space. COW calculates the linear factors by a simple matrix multiplication performed in the Logic *PCATransform*.

D Visual Inspection of the Eigenvectors

To decide which conformational transitions are captured by the eigenvectors, one needs to visually inspect them. Therefore, trajectories are simulated along one eigenvector. The algorithm for the generation of trajectories is implemented as *TrajectoryVisualizer* in CowEyes. It shows the information represented by a single user-specified eigenvolume by simulating a trajectory of N volumes. From the linear factors calculated in *PCATransform* one could retain each volume V_n in the dataset through the relation

$$V_n = \bar{V} + \sum_{k=1}^K a_{nk} E_k \quad (1)$$

where \bar{V} is the average volume calculated in the PCA, V_n is the n -th volume in the ensemble, E_k is the k -th eigenvolume describing a conformational motion and a_{nk} are the linear factors that act as coordinates of V_n in the space spanned by E_k .

TrajectoryVisualizer simulates a series of volumes that only displays the information encoded by a single eigenvolume E_k . Hence Eq. 1 simplifies to

$$V_k = \bar{V} + a_k E_k. \quad (2)$$

To show the N snapshots along the trajectory, first the linear factors of all volumes with respect to the specified eigenvector E_k are collected and sorted into one vector $a_k = (a_{1k}, \dots, a_{Nk})^T$, where a_{1k} and a_{Nk} are the smallest and largest linear factors, respectively. The number of principal components is $K \leq N$, because typically the size of the volume (i.e. the number of voxels) is larger than the size of the ensemble (i.e. the number of volumes). The average volume \bar{V} is constant throughout the dataset. *TrajectoryVisualizer* now offers two modes: Either the real linear factors are used for the calculation (i.e. all elements of a_k) or an equally sampled interval between a_{1k} and a_{Nk} is used. In the latter case, a trajectory sampled with a stepsize of $(a_{Nk} - a_{1k})/(N - 1)$ is visualized. By applying Eq. (2) for each element in the vector a_k , or for each sample in the interval $[a_{1k}, a_{Nk}]$, respectively, a volume series is calculated. The snapshot volumes along the trajectory can be visualized in the Volume viewer of CowEyes. Supplementary Videos were generated by loading the full trajectory into UCSF Chimera and recording a movie of a morph between the snapshots (a Chimera script is provided in the supplement).

E Energy Landscape Estimation

The previous analysis steps mainly serve us to find an efficient representation of the input 3D volumes in a low-dimensional space. What is still missing is a continuous description of this space that also allows the estimation of energy differences between ensemble members. The algorithm for the estimation of a continuous surface from the linear factor representation is also implemented in CowEyes as *EnergyLandscape*. From two chosen eigenvolumes E_1 and E_2 , the linear factors are saved in two vectors $a_1 = (a_{11}, \dots, a_{N1})^T$ and $a_2 = (a_{12}, \dots, a_{N2})^T$, respectively. Additionally, a third vector $c = (c_1, \dots, c_N)^T$ containing the observation frequencies or particle counts of the corresponding volume is stored. Each data point of the form (a_{n1}, a_{n2}, c_n) is then mapped to a grid forming a weighted point cloud. To estimate a continuous surface, kernel density estimation (KDE) with a Gaussian kernel function

$$\phi_n(x, y) = c_n e^{-\frac{1}{2\sigma^2}((x-a_{n1})^2+(y-a_{n2})^2)}$$

is used where x and y are the centers of the cells of the sampling grid. The Gaussian kernels are evaluated at each grid point (x, y) and added together resulting in a continuous probability surface:

$$\phi(x, y) = \sum_n \phi_n(x, y) = \sum_n c_n e^{-\frac{1}{2\sigma^2}((x-a_{n1})^2+(y-a_{n2})^2)} \quad (3)$$

The bandwidth σ determines the width of the Gaussian and has to be user-adjusted. With the standard grid spacing, all landscapes shown are plotted with a σ of 300px. An energy landscape is obtained by computing $-\log \phi(x, y)$, which follows from Boltzmann inversion. Alternatively, we can use Gaussian kernel regression to approximate the energy landscape directly by relating the counts in (Eq. 3) with temperature-normalized Gibb's free energies:

$$\left(\frac{\Delta G}{k_B T}\right)_n = \ln \left(\frac{c_n}{\max\{c_n\}}\right)$$

A final 3D-rendered visualization of the landscape can be obtained by CowEyes' built-in surface viewer, which is based on the Qt Data Visualization library.